

This article may be downloaded for personal use only. Any other use requires prior permission of the author and American Society for Microbiology.

The following article appeared in *Applied and Environmental Microbiology*, June 2017 vol. 83 no. 11 e00645-17; and may be found at <https://dx.doi.org/10.1128/AEM.00645-17>

1 **Anaerobic methane oxidation driven by microbial reduction of natural organic matter**
2 **in a tropical wetland**

3

4 Edgardo I. Valenzuela¹, Alejandra Prieto-Davó², Nguyen E. López-Lozano¹, Alberto
5 Hernández-Eligio³, Leticia Vega-Alvarado⁴, Katy Juárez³, Ana Sarahí García-González⁵,
6 Mercedes G. López⁵ & Francisco J. Cervantes^{1,*}

7

8 1. División de Ciencias Ambientales, Instituto Potosino de Investigación Científica y
9 Tecnológica. Camino a la Presa San José 2055 Col. Lomas 4ª. Sección, San Luis Potosí,
10 SLP 78216 Mexico.

11 2. Facultad de Química, Unidad Sisal, Universidad Nacional Autónoma de México. Puerto
12 de Abrigo s/n, Sisal, Yucatán, 97356 Mexico.

13 3. Departamento de Ingeniería Celular y Biocatálisis, Instituto de Biotecnología,
14 Universidad Nacional Autónoma de México, Campus Morelos. Av. Universidad 2001,
15 Cuernavaca Morelos, 62210 Mexico.

16 4. Centro de Ciencias Aplicadas y Desarrollo Tecnológico, Universidad Nacional
17 Autónoma de México, Circuito exterior s/n, Ciudad Universitaria, Coyoacán, D.F., 04510
18 Mexico.

19 5. Departamento de Biotecnología y Bioquímica, Centro de Investigación y de Estudios
20 Avanzados del IPN, Unidad Irapuato, Irapuato, Mexico.

21

22 Running title: Anaerobic methane oxidation linked to humus reduction

23 Keywords: Anaerobic methane oxidation, humus, methanotrophy, wetlands

24 *Corresponding author: Francisco J. Cervantes, fjcervantes@ipicyt.edu.mx

25 **Abstract**

26 Wetlands constitute the main natural source of methane on Earth due to their high content
27 of natural organic matter (NOM), but key drivers such as electron acceptors supporting
28 methanotrophic activities in these habitats are poorly understood. We performed anoxic
29 incubations using freshly collected sediment along with water samples harvested from a
30 tropical wetland, amended with ^{13}C -methane (0.67 atm) to test the capacity of its microbial
31 community to perform anaerobic methane oxidation (AOM) linked to the reduction of the
32 humic fraction of its NOM. Collected evidence demonstrates that electron-accepting
33 functional groups (*e.g.* quinones) present in NOM fueled AOM by serving as terminal
34 electron acceptor. Indeed, while sulfate reduction was the predominant process accounting
35 for up to 42.5% of the AOM activities, microbial reduction of NOM concomitantly
36 occurred. Furthermore, enrichment of wetland sediment with external NOM provided
37 complementary electron-accepting capacity, which reduction accounted for $\sim 100 \text{ nmol } ^{13}\text{C}$ -
38 CH_4 oxidized $\text{cm}^{-3} \text{ d}^{-1}$. Spectroscopic evidence showed that quinone moieties were
39 heterogeneously distributed in the wetland sediment, and that their reduction occurred
40 during the course of AOM. Moreover, an enrichment derived from wetland sediments
41 performing AOM linked to NOM reduction stoichiometrically oxidized methane coupled to
42 the reduction of the humic analogue, anthraquinone-2,6-disulfonate. Microbial populations
43 potentially involved in AOM coupled to microbial reduction of NOM were dominated by

44 divergent biota from putative AOM-associated archaea. We estimate that this microbial
45 process could potentially contribute to the suppression of up to 114 Tg CH₄ yr⁻¹ in coastal
46 wetlands and more than 1,300 Tg yr⁻¹ considering the global wetland area.

47

48 **Importance**

49 Identifying key processes governing methane emissions from natural systems is of major
50 importance considering the global warming effects triggered by this greenhouse gas. AOM
51 coupled to the microbial reduction of distinct electron acceptors plays a pivotal role in
52 mitigating methane emissions from ecosystems. Given their high organic content, wetlands
53 constitute the largest natural source of atmospheric methane. Nevertheless, processes
54 controlling methane emissions in these environments are poorly understood. Here we
55 provide tracer analysis with ¹³CH₄ and spectroscopic evidence revealing that AOM linked
56 to the microbial reduction of redox functional groups in natural organic matter (NOM)
57 prevails in a tropical wetland. We suggest that microbial reduction of NOM may largely
58 contribute to suppress methane emissions from tropical wetlands. This is a novel avenue
59 within the carbon cycle in which slowly decaying NOM (*e.g.* humic fraction) in
60 organotrophic environments fuels AOM by serving as terminal electron acceptor.

61

62

63

64

65

66 Introduction

67 Microbial processes produce and consume methane (CH₄) in anoxic sediments playing a
68 crucial role in regulating Earth's climate. Virtually 90% of CH₄ produced from marine
69 environments is oxidized by microorganisms avoiding its release to the atmosphere (1).
70 Anaerobic oxidation of methane (AOM) associated with sulfate reduction was first
71 discovered in marine environments (2). More recently, AOM has also been linked to the
72 microbial reduction of nitrate (3, 4) and nitrite (5), as well as Fe(III) and Mn(IV) oxides (6–
73 8) in freshwater and marine environments. Wetlands are the largest natural source of CH₄
74 (9), contributing to about a third of global emissions (10), but key drivers, such as electron
75 acceptors fueling methanotrophic activities in these habitats, are poorly understood. CH₄
76 emissions from wetlands have been strongly responsive to climate in the past, and will
77 likely continue to be responsive to anthropogenic-driven climate change in the future,
78 predicting a large impact on global atmospheric CH₄ concentration (10). The traditional
79 assumption is that aerobic methanotrophy dominates wetlands' CH₄ cycling by oxidizing
80 an estimated 40 to 70% of gross CH₄ production in these ecosystems (11). Recent findings
81 (12) challenged this conjecture by providing evidence that AOM may consume up to 200
82 Tg CH₄ yr⁻¹, decreasing their potential CH₄ emission by 50% in these habitats. Most AOM
83 activities observed in wetlands have been related to sulfate reduction (12, 13), but other
84 electron acceptors remain feasible. Natural organic matter (NOM), circumscribed to humic
85 substances (HS) in many studies (14), occurs at high concentrations in wetlands both in
86 soluble and solid phases (15). Recent evidence indicates that HS suppress methane
87 production in different ecosystems (16, 17), yet the mechanisms involved are still
88 enigmatic. HS can theoretically promote AOM as they can serve as terminal electron

89 acceptors for microbial respiration (18, 19) and have higher redox potential than sulfate
90 (20). However, compelling evidence demonstrating AOM driven by the microbial reduction
91 of NOM present in anoxic environments remains elusive (21, 22).

92 We aimed to document $^{13}\text{CH}_4$ anaerobic oxidation and the ongoing reduction of intrinsic
93 electron acceptors, including the electron accepting fraction of NOM, by the biota of
94 freshly sampled sediment from a coastal tropical wetland. We provide $^{13}\text{CH}_4$ tracer studies
95 and spectroscopic evidence demonstrating for the first time that AOM is linked to the
96 microbial reduction of redox functional groups present in the NOM of this tropical marsh.
97 Furthermore, we found evidence, based on 16S rRNA gene sequences, indicating that
98 microbial populations potentially involved in AOM coupled to microbial reduction of
99 NOM were dominated by divergent biota from putative AOM-associated microorganisms.

100

101 **Results**

102 **Kinetics of ^{13}C -methane oxidation and electron balances**

103 Exponential phase of AOM was observed in microcosms over the first 15 days of
104 incubation in the case of unamended sediment (free from external NOM addition). The
105 methanotrophic rate in this experimental treatment was $\sim 1.34 \mu\text{mol } ^{13}\text{C}\text{-methane oxidized}$
106 $\text{cm}^{-3} \text{d}^{-1}$ (Fig. 1). At the end of the exponential phase, sulfate and Fe(III) reduction
107 accounted for 42.5% and 0.5% of ^{13}C -methane oxidized, respectively, while the role of
108 nitrate was marginal (Fig. 2 and Table S2). These unamended sediment microcosms
109 exhibited a reduction in intrinsic NOM during the course of AOM, which was expected due
110 to the high concentration of organic carbon in the tropical wetland, with the capacity to

111 accept electrons (Table S1, Fig. 2). Nevertheless, large perturbation caused by endogenous
112 NOM reduction in experimental controls lacking ^{13}C -methane obstructed accurate
113 assessment of AOM driven by this microbial process (Fig. 2). The large endogenous NOM
114 reduction observed in these control experiments may be explained by concomitant methane
115 production (and subsequent consumption) observed (Fig. S2), and by oxidation of labile
116 organic matter present in the sediment (Table S1). Supplementary incubations spiked with
117 the sulfate-reduction inhibitor, sodium molybdate (25 mM), showed decreased sulfate
118 reducing activities ($\sim 50\%$, Fig. 2), while AOM rates remained high when compared against
119 their non-inhibited counterparts (Fig. 1). Remarkably, when sulfate reduction was inhibited,
120 the reduction of intrinsic NOM was doubled (from 1.6 ± 0.11 to 3.4 ± 0.19 milli-electron
121 equivalents (meq) l^{-1}), implying that the reduction of redox functional groups in NOM was
122 promoted when the utilization of sulfate was impeded.

123 Further enrichment of wetland sediment with external NOM, in the form of HS derived
124 from *Pahokee Peat* (Florida Everglades, 2.5 g l^{-1}), provided complementary electron
125 accepting capacity, which significantly elicited AOM up to $\sim 1.88 \mu\text{mol } ^{13}\text{C}$ -methane
126 oxidized $\text{cm}^{-3} \text{ d}^{-1}$ and extended the exponential phase to 20 days (Fig. 1). In this
127 experimental treatment, electron balances revealed a methanotrophic activity responsible of
128 $\sim 100 \text{ nmol } ^{13}\text{C}\text{-CH}_4$ oxidized $\text{cm}^{-3} \text{ d}^{-1}$ linked to microbial reduction of NOM (including
129 both intrinsic and externally added as *Pahokee Peat* HS). As hypothesized before,
130 consumption of intrinsically produced methane was confirmed by experimental controls
131 enriched with HS from *Pahokee Peat* and incubated in the absence of ^{13}C -methane, which
132 showed significant consumption of $^{12}\text{CH}_4$ (Fig. S2). This was also confirmed by increased
133 $^{12}\text{CO}_2$ production quantified, which was reflected on 2 to 4-fold lower enrichment of $^{13}\text{CO}_2$

134 in HS enriched incubations as compared to unamended controls (see $^{13}\text{FCO}_2$ values in Fig.
135 1). Reports (23, 24) indicate that methanotrophic microorganisms prefer to oxidize $^{12}\text{CH}_4$ as
136 compared to $^{13}\text{CH}_4$, which may partly explain our findings.

137 The role of sulfate reduction on AOM when wetland sediment was enriched with HS was
138 not possible to assess (Table S2) due to large endogenous sulfate reduction elicited by
139 degradation of the labile fraction of externally added NOM (Fig. 2), which also triggered
140 methanogenesis in these microcosms. Since no significant differences in iron reduction
141 were detected between microcosms with or without $^{13}\text{CH}_4$ addition, the only microbial
142 process clearly identified driving AOM in *Pahokee Peat* enriched sediments was the
143 microbial reduction of HS (Table S2).

144 **Spectroscopic evidence on presence and reduction of redox-functional groups in NOM**

145 Initial exploration of the solid phase NOM present in wetland sediment by micro-ATR-
146 FTIR spectra, revealed the presence of electron accepting moieties both in unamended and
147 in HS enriched wetland sediments. By mapping of acquisition points at 1650-1620 cm^{-1} ,
148 presence and heterogeneous distribution of quinone functional groups was evidenced in
149 sediments confirming the presence of non-soluble electron accepting moieties classically
150 attributed to humic-like materials (Fig. 3a and b). To further confirm this, we looked for
151 double bonded carbon and oxygen (C=O) by use of X-ray photoelectron spectra (XPS),
152 technique that supported the existence of quinone-like functional groups in unamended
153 sediment and furthermore, provided evidence of the reduction of these moieties by showing
154 the disappearance of the C=O signal from C1s and O1s high resolution spectra when
155 comparing signals from sediment analyzed before and after incubation with $^{13}\text{CH}_4$ in the

156 absence of external HS (Fig. 3c to f). Another missing signal after the AOM process was
157 that which corresponds to metallic oxides, evidenced by analysis of the O1s high resolution
158 spectra (Figure 3d and f), which may imply reduction of intrinsic iron oxides that supported
159 ~0.5% of methanotrophy according to electron balances (Table S2). Further analysis of the
160 liquid phase of pristine sediment microcosms also revealed the reduction of quinone-like
161 moieties during the course of AOM (Fig. 4). Initial samples exhibited a well-defined and
162 strong peak at 1690 cm⁻¹ associated with quinone moieties, while reduced samples, at the
163 end of the incubation period, showed an increase in the signal related to phenolic groups
164 (1660 cm⁻¹). Additional signals of phenolic groups were detected after incubation with
165 ¹³CH₄ and *Pahokee Peat* by spectral signals detected around 2260-2500 cm⁻¹ (25).

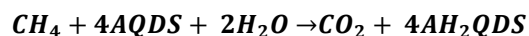
166 **Microbial communities performing AOM**

167 According to 16S rRNA gene sequences from wetland sediment samples performing AOM,
168 anaerobic methanotrophic archaea (ANME), which are traditionally linked to anaerobic
169 methanotrophy under sulfate-reducing (2, 26), Fe(III)-reducing (6, 8), and artificial electron
170 acceptor-reducing conditions (27), were barely detected in our experiments, with ANME-
171 1b and ANME-3 representing less than 0.5% and 0.2%, respectively, from the archaeal
172 community in all experimental treatments (Fig. 5). The only abundant *Euryarchaeota*
173 members detected were affiliated to an unclassified genus of the Marine Benthic Group D
174 family (MBGD and DHVEG-1), which accounted for 18 to 23% of the archaeal biota in all
175 treatments. Outside of the *Euryarchaeota* phylum, members from the newly named
176 *Bathyarchaeota* lineage (formerly known as Miscellaneous Crenarchaeotic Group) were
177 another cluster of microorganisms that remained in high percentages (from 8 to 14%) in all
178 treatments. Two genera from the *Thaumarchaeota* phylum, one belonging to the

179 pMC2A209 class, and the other from the Marine Benthic Group B (MBG-B) were also
180 consistently present in all sediment samples showing AOM, the latter one increasing its
181 proportion up to 12% when sulfate reduction was inhibited (Fig. 5). From the bacterial
182 counterpart, the most abundant bacteria in two of the treatments was a genus of
183 *Oceanimonas* from *Aeromonadaceae* family (*Gammaproteobacteria*), whose presence was
184 diminished when sulfate reduction was inhibited and when $^{13}\text{CH}_4$ was absent (Fig. S3),
185 suggesting that this microorganism might have been involved in sulfate-dependent AOM.
186 Other evident changes in the bacterial community included the increase of *Clostridia* and
187 *Bacilli* members when external NOM was supplied (Fig. S3), which agrees with their
188 capacity to reduce HS (28).

189 **AOM linked to AQDS reduction**

190 In order to confirm the capacity of the sediment biota to channel ^{13}C -methane derived
191 electrons to quinone groups, the humic analogue, anthraquinone-2,6-disulfonate (AQDS),
192 was added as an electron acceptor to the artificial basal medium for sediment enrichments.
193 AQDS reduction and methane consumption were observed since the first enrichment cycle,
194 although no clear relationship between net methane consumption and AH_2QDS production
195 was observed due to high concentrations of intrinsic electron donors and acceptors (data not
196 shown). Nevertheless, during the third incubation cycle, net AOM was observed within 11
197 days, which corresponded to a final ratio of oxidized methane/reduced AQDS of 1:4.7
198 corrected for endogenous controls, which is very close to the stoichiometric 1:4 according
199 to the following equation (Fig. 6a):



200 **Gibbs free energy (ΔG°) = -43.2 kJ mol⁻¹**

201 Analysis of 16S rRNA gene sequences from enriched sediment sampled at the end of the
202 third cycle of AQDS-dependent AOM activity (Fig. S1) displayed a significant decrease on
203 the diversity of the microbial community evidenced by a decrease in Shannon index, from
204 5.52 in freshly sampled sediment to 3.56 after enrichment with CH₄ and AQDS. Significant
205 increments and decreases of specific groups of archaea and bacteria did occur in this
206 enrichment (Fig. 6b and c). From the archaeal fraction, the pMC2A209 class from the
207 *Thaumarchaeota* and the *Methanosaeta* genera were archaeal clusters that significantly
208 increased their presence in the AQDS enrichment (34% and 23%, respectively). Also in the
209 AQDS enrichment, the *Bathyarchaeota* phylum previously detected in wetland sediments,
210 both in the presence and in the absence of external NOM, significantly increased its
211 proportion in the archaeal community (around 10% respect to the original composition),
212 suggesting potential metabolic arrangements to thrive under AQDS-dependent AOM
213 conditions (Fig. 6b). Humus-reducing bacteria that proliferated throughout the five months
214 of enrichment included genera from the *Desulfuromonadales* (29, 30), *Clostridiales* (14,
215 28) and *Propionibacteriales* (31) orders in 27%, 7%, and 12%, respectively, with respect
216 to the original composition (Fig. S3).

217

218 **Discussion**

219 **NOM as terminal electron acceptor fueling AOM in wetland sediment.** Although the
220 complex composition of the studied wetland sediment challenged efforts to elucidate the
221 microbial processes responsible for the high methanotrophic activities quantified, the

222 present study provides multiple lines of evidence demonstrating that electron-accepting
223 functional groups present in its NOM fueled AOM by serving as terminal electron acceptor.
224 Indeed, while sulfate reduction was the predominant process accounting for up to 42.5% of
225 AOM activities, microbial reduction of NOM concomitantly occurred. Furthermore,
226 enrichment of wetland sediment with external NOM, as *Pahokee Peat* HS, significantly
227 promoted AOM with a quantified amount of $\sim 100 \text{ nmol } ^{13}\text{C-CH}_4 \text{ oxidized cm}^{-3} \text{ d}^{-1}$
228 attributed to this microbial process. Spectroscopic evidence also demonstrated that quinone
229 moieties, main redox functional groups in HS (19), were heterogeneously distributed in the
230 studied wetland sediment and that their reduction occurred during the course of AOM.
231 Moreover, an enrichment derived from wetland sediments performing AOM linked to
232 NOM reduction stoichiometrically oxidized methane coupled to AQDS. Sediment
233 incubations performed in the presence of the sulfate reduction inhibitor, molybdate, further
234 confirmed the role of HS in AOM. Certainly, even though sulfate-reducing activities
235 significantly decreased in the presence of molybdate, AOM activities remained high, while
236 microbial reduction of NOM was doubled under these conditions. These interesting
237 findings suggest that methanotrophic microorganisms performing sulfate-dependent AOM
238 might have directed electrons derived from AOM towards NOM when sulfate reduction
239 became blocked as has been suggested based on experiments performed under artificial
240 conditions (27).

241 **Microbial communities in wetland sediments performing AOM.** Archaeal clusters
242 consistently found in wetland sediment incubations performing AOM included members
243 from the MBG-D family, which have already been proposed as players in metal-dependent
244 AOM (6), thus their presence agrees with evidence indicating AOM linked to iron

245 reduction observed in some experimental controls (Table S2). Additionally, these
246 microorganisms were not found in the AQDS enrichment, probably due to depletion of
247 intrinsic ferric iron throughout the incubation cycles. Archaea constantly present amongst
248 fresh sediment incubation and AQDS enrichment were those from the pMC2A209 class
249 and the *Bathyarchaeota* phylum. To our knowledge, the pMC2A209 class of archaea has
250 not been related to AOM, but its close partners from the MBG-B class have been
251 consistently found in environments in which AOM occurs (32–35). In fact,
252 *Thaumarchaeota* members, including the MBG-B, have been found in consortia
253 performing AOM in the absence of ANME clades (36). Interestingly, the pMC2A209
254 cluster seemed to duplicate its proportion up to 12% when sulfate reduction was inhibited
255 (by molybdate), which might suggest that the impediment of sulfate reduction enhanced its
256 activity promoting AOM coupled to NOM reduction. Respect to the *Bathyarchaeota*
257 phylum, increasing evidence suggests that this lineage might be involved in the methane
258 cycle. Recently, it has been demonstrated that this cluster possesses the necessary genetic
259 elements to express the enzymatic machinery required for methane production, and
260 potentially methane consumption (37). Additionally, Saxton and colleagues have found
261 abundant *Bathyarchaeota* representation in a fulvic acids rich deep sediment that oxidizes
262 methane uncoupled from sulfate reduction (22). Unexpectedly, a very low percentage
263 within the archaeal population was identified as members from the ANME type archaea,
264 even though it would be expected to find ANME-2 members since it is the only ANME
265 subgroup with proven capability to derive electrons extracellularly towards humus and its
266 analogues under artificial conditions (27). Our microcosms, both in fresh sediment as well
267 as in the AQDS long-term enrichment, showed a barely detectable number of copies of

268 ANME-1b and ANME-3 sequences retrieved by the methodology employed, suggesting a
269 low presence of ANME microorganisms in the ecosystem studied.

270 Regarding the bacterial composition, while *Clostridia*, *Bacilli* and *Gammaproteobacteria*
271 were significantly represented within the fresh sediment performing AOM (Fig. S3), the
272 AQDS enrichment (Fig. 6) exhibited the most significant increase in *Deltaproteobacteria*
273 of the *Desulfuromonadales* order, which includes several humus-reducing microorganisms
274 (14). Since a wide diversity of microorganisms have been proven to reduce humus
275 analogues or HS, we do not rule out that diverse bacterial clusters could have participated
276 in partnership with detected archaea to jointly performed AOM coupled to NOM reduction.
277 Nevertheless, humus-reducing bacteria possess metabolic versatility and capability to
278 reduce miscellaneous electron acceptors, which makes it difficult to come to conclusions
279 about their participation in our experiments. Further investigation must be done to unravel
280 the potential involvement of humus-reducing bacteria in AOM.

281 **Ecological significance.** To our knowledge this is the first report of AOM coupled to
282 microbial reduction of NOM, which constitutes a missing link within the carbon cycle. HS
283 frequently contribute up to 80% of soil NOM and up to 50% of dissolved NOM in aquatic
284 environments. While the labile fraction of NOM promotes methanogenesis in anaerobic
285 environments, the slowly decomposing humic portion may serve as an important barricade
286 to prevent methane emissions in organotrophic ecosystems by serving as terminal electron
287 acceptor driving AOM (Fig. 7). As an example, considering the maximum AOM driven by
288 microbial reduction of NOM measured in humic enriched sediments, and the global area of
289 coastal wetlands (38, 39), we approximate that this microbial process consumes up to 114
290 Tg CH₄ yr⁻¹. Considering the global wetland area (10), we anticipate methane suppression

291 of more than 1,300 Tg yr⁻¹ (see Supplemental Material for details). Accordingly, NOM-
292 driven AOM may be more prominent in organotrophic sites with poor sulfate content, such
293 as peatlands, swamps and organotrophic lakes. This premise is supported by suppression of
294 methanogenesis by HS observed in different ecosystems (16, 17) and by the widespread
295 AOM activity reported across many peatland types (40–42). The potential role of HS is
296 further emphasized because their electron accepting capacity is fully recycled in recurrently
297 anoxic environments. Thus, the suppression of methanogenesis by HS estimated to be of
298 the order of 190,000 mol CH₄ km⁻² yr⁻¹ may be much larger than previously considered
299 (43).

300

301 **Materials and Methods**

302 **Sediment sampling and characterization**

303 Sediment cores were collected from the tropical marsh *Sisal*, located in Yucatán Peninsula,
304 south-eastern Mexico (21°09'26''N, 90°03'09''W) in January 2016. Sediment cores with a
305 depth of 15 cm were collected under a water column of approximately 70 cm. Water
306 samples were also collected from the area of sediment sampling points to be used as liquid
307 medium in anaerobic incubations. All sediment and water samples were sealed in hermetic
308 flasks and were maintained in ice until arrival to the laboratory. Upon arrival, all sampled
309 materials were stored at 4°C in a dark room until analysis and incubation. Sediment cores
310 were opened and homogenized within an anaerobic chamber (atmosphere composed of
311 N₂/H₂ (95%/5%, v/v)) before characterization and incubation. No amendments (addition of
312 chemicals, washing or exposure to air) were allowed on sediment and water samples in

313 order to reflect the actual conditions prevailing *in situ* as closely as possible.
314 Characterization of water and sediment samples is described in Table S1.
315

316 **Sediment incubations.** Water samples collected from sediment sampling points were
317 thoroughly mixed before amendment with HS (2.5 g l⁻¹) by magnetic stirring. *Pahokee Peat*
318 (Florida, Everglades) HS, purchased from the International Humic Substances Society,
319 were employed as external NOM in sediment incubations. Humic-enriched water was
320 flushed with N₂ to blow away any dissolved oxygen. Portions of 15 ml were then
321 distributed in 25-ml serological flasks. Sediment containers were opened inside an
322 anaerobic chamber. Portions of 2.5 ml of wet sediment previously homogenized were then
323 inoculated into each serological bottle. After sealing all bottles with rubber stoppers and
324 aluminum rings inside the anaerobic chamber, they were flushed with N₂. Once anaerobic
325 conditions were established, 5 ml of ¹³C-labeled methane were injected into each vial to
326 reach a ¹³CH₄ partial pressure of 0.67 atm in a headspace of 7.5 ml. Controls incubated in
327 the absence of external HS were also prepared by following an identical protocol. Killed
328 controls included chloroform at a concentration of 10% (v/v) to annihilate any microbial
329 activity. Additional incubations were executed in the presence of the sulfate-reduction
330 inhibitor, molybdate (25 mM), in the presence and in the absence of external NOM. All
331 incubation bottles were statically placed in a dark room at 28 °C (temperature prevailing at
332 *Sisal* wetland at the sampling time). The pH remained at 7.5±0.05 throughout all
333 incubations.

334 **Enrichment incubations with AQDS.** Incubations were commenced by inoculating 120-
335 ml serological bottles with 10 g of volatile suspended solids (VSS) l⁻¹ of *Sisal* sediment.

336 Prior inoculation, portions of 60 ml of artificial medium were distributed into the
337 incubation bottles and flushed for 15 min with a mixture of N₂:CO₂ (80%/20%, v/v) for
338 stripping any dissolved oxygen from the medium. AQDS (>98.0% purity, TCI AMERICA
339 Chemicals) was added at a concentration of 10 mM as terminal electron acceptor along
340 with the following basal medium components (g l⁻¹): NaHCO₃ (5), NH₄Cl (0.3), K₂HPO₄
341 (0.2), MgCl₂·6H₂O (0.03) and CaCl₂ (0.1). Trace elements were included in the medium by
342 adding 1 ml l⁻¹ of a solution with the following composition (mg l⁻¹): FeCl₂·4H₂O (2,000),
343 H₂BO₃ (50), ZnCl₂ (50), CuCl₂·6H₂O (90), MnCl₂·4H₂O (500), AlCl₃·6H₂O (90),
344 CoCl₂·6H₂O (2000), NiCl₂·6H₂O (920), Na₂SeO₄·5H₂O (162), (NH₄)₆Mo₇O₂₄ (500), EDTA
345 (1,000), Na₂WO₄·H₂O (100) and 1 ml l⁻¹ of HCl at 36%. The final pH of the medium was
346 7.2 and no changes were observed throughout the incubation time. Once inoculation took
347 place, microcosms were sealed with rubber stoppers and aluminum rings, and then flushed
348 with the same N₂:CO₂ mixture. After anoxic conditions were established, 1 ml of sodium
349 sulfide stock solution was injected into each vial to reach a sulfide concentration of 0.1 g l⁻¹
350 in order to consume any traces of dissolved oxygen. Methane was provided into the
351 microcosms by injecting 30 ml of CH₄ (99.9% purity, Praxair) reaching a partial pressure of
352 methane of 0.54 atm. Subsequent incubations were performed after AQDS was reduced
353 (converted to AH₂QDS) coupled to anaerobic oxidation of methane (AOM). A new set of
354 bottles containing basal medium with AQDS (10 mM) were inoculated within an anaerobic
355 chamber by transferring 10 ml of slurry (sediment and medium) taken from previous
356 incubations (Fig. S1). The following incubations were completed under the same
357 experimental conditions.

358 **Analytical techniques**

359 **Isotopic carbon dioxide and methane measurements.** Ions 16 ($^{12}\text{CH}_4$), 17 ($^{13}\text{CH}_4$), 44
360 ($^{12}\text{CO}_2$) and 45 ($^{13}\text{CO}_2$) were detected and quantified in a Gas Chromatograph Agilent
361 Technologies 7890A coupled to a Mass Spectrometer (detector) Agilent Technologies
362 5975C, the ionization was achieved by electronic impact and quadrupole analyzer. For the
363 analysis, a capillary column Agilent Technologies HP-PLOT/Q with a stationary phase of
364 poly-styrene-di-vinyl-benzene ($30\text{ m} \times 0.320\text{ mm} \times 20\text{ }\mu\text{m}$) was employed as stationary
365 phase using helium as carrier gas. The chromatographic method was as follows: the starting
366 temperature was $70\text{ }^\circ\text{C}$ which was held for 3 min, and then a ramp with an increase of $20\text{ }^\circ\text{C}$
367 per min was implemented until $250\text{ }^\circ\text{C}$ was reached and maintained for 1 min. The total
368 time of the run had a duration of 13 min. The temperature of the injection port was $250\text{ }^\circ\text{C}$.
369 The injection volume was $20\text{ }\mu\text{l}$ and there was only one replicate of injection per bottle. The
370 gas injected into the GC was taken directly from the headspace of the incubations and
371 immediately injected in to the GC port. Methane calibration curves were made by injection
372 of different methane (99.9% of purity) volumes into serological bottles under the same
373 experimental conditions (atmosphere composition, pressure, temperature, and liquid
374 volume). $^{12}\text{CO}_2$ and $^{13}\text{CO}_2$ curves were made using different dried sodium bicarbonate
375 (99% purity, Sigma Aldrich) and sodium ^{13}C -labelled carbonate (99 atom % ^{13}C , Sigma
376 Aldrich) concentrations, respectively, in serological bottles which contained the same
377 volume of wetland sediment and water used in incubations. Standards were incubated at
378 room temperature for 12 hours until equilibrium with the gaseous phase was reached. The
379 linear regression analysis of obtained measurements had a co-relation coefficient higher
380 than 0.97. $^{13}\text{CO}_2$ production rates were based on the maximum slope observed on linear
381 regressions considering at least three sampling points.

382 **Methane quantification in AQDS enrichment.** Net methane consumption was assessed in
383 terms of methane concentration measurements in the headspace of microcosms. These
384 measurements were carried out by injecting 100 μ l of gas samples from the headspace of
385 incubation bottles into a gas chromatograph (Agilent Technologies 6890M) equipped with
386 a thermal conductivity detector, and a Hayesep D (Alltech, Deerfield, Illinois, USA)
387 column with the following dimensions: 3.048 m \times 3.185 m \times 2.16 mm. Helium was
388 employed as carrier gas at a flux of 12 ml min⁻¹. The temperature of injection port, oven
389 and detector was 250, 60 and 250 °C, respectively. Calibration curves were made for each
390 reaction volume used by injecting different methane concentrations into serological bottles
391 under the same experimental conditions at which microcosms were performed (atmosphere
392 composition, pressure, temperature, and liquid volume).

393 **Determination of electron accepting functional groups in solid phase by XPS.**

394 Sediment samples (solid fraction of microcosms) were dried under a constant nitrogen flow
395 after incubation with methane. Once sediments became dried, bottles were open inside an
396 anaerobic chamber with an atmosphere composed of N₂/H₂ (95%/5%, v/v) and were
397 triturated on an agate mortar. Samples were then kept under anaerobic conditions until
398 analysis in a X-Ray Photoelectron Spectroscopy Analyzer PHI VersaProbe II (Physical
399 Electronics, ULVAC-PHI). Two representative spectra were recorded per scanned sample.

400 **Determination of electron accepting functional groups in solid phase by Micro-ATR-**

401 **FT-IR imaging.** Micro-ATR-FT-IR images were collected from each sample with a
402 continuous scan spectrometer, Agilent 660 FT-IR interfaced to a 620 infrared microscope
403 with a 32 \times 32 FPA detector and Ge ATR objective for micro-ATR. Each pixel obtains a
404 full IR spectrum or a total of 1024 spectra. Background spectra were collected from a clean

405 ATR crystal (i.e., without sample). The Ge crystal of the ATR microscope was lowered
406 onto the surface of each sample for a contact area of approximately $100 \times 100 \mu\text{m}$. Spectra
407 were collected by co-addition of 256 scans over a spectral range of 4000 to 900 cm^{-1} , at a
408 spectral resolution of 4 cm^{-1} . In all images, a color scale bar is set within the software to
409 reflect the relative concentration range, from low to high. Agilent Resolutions Pro was used
410 for data acquisition and analysis.

411 **Determination of electron accepting functional groups in liquid phase by high**
412 **resolution UV-Vis-NIR spectroscopy.** After each incubation cycle, liquid samples (1.5
413 ml) were taken in an anaerobic chamber with a disposable syringe and put into a quartz
414 cell, which was sealed with plastic film in order to keep anoxic conditions during
415 spectrometric analysis. Spectra were obtained in a Varian Cary 5000 UV-Vis (diffuse
416 reflectance) spectrophotometer, equipped with an integrating sphere.

417 **Nitrite and nitrate determinations.** Nitrite and nitrate concentrations were measured
418 according to spectrometric techniques established at Standard Methods (44). Nitrate
419 measurement is taken under acidic conditions at a wavelength of 275 nm and the value
420 obtained is corrected for dissolved organic matter which has its maximum absorbance at
421 220 nm . Nitrite forms a purple complex through a reaction with sulfanilamide and N-(1-
422 naphthyl) ethylene diamine, which presents its maximum absorbance at a wavelength of
423 543 nm . Samples were taken with a disposable syringe directly from the microcosms,
424 injected into sealed quartz cuvettes or glass tubes (depending on the required lecture
425 wavelength) and immediately taken to the spectrophotometer to avoid any reaction of the
426 sample with atmospheric oxygen.

427 **Sulfate and sulfide determinations.** Samples were extracted from microcosms and
428 immediately filtered through 0.22 μm nitrocellulose membranes. Filtered samples were
429 then diluted (1:10) with deionized water and processed in an Agilent Capillary
430 Electrophoresis System (Agilent Technologies) according to the methodology proposed by
431 Soga & Ross (45). Dissolved sulfide was measured by the spectrometric method proposed
432 by Cord-Ruwisch (46). Briefly, 100 μl of sample were taken and immediately mixed in
433 vortex with 4 ml of an acidic CuSO_4 solution. Absorbance at 480 nm was immediately
434 registered in a UV-VIS spectrophotometer (Thermo Spectronic) to avoid sulfide oxidation
435 before measurements.

436 **Humic substances reduction and ferrous iron measurements.** Quantification of the
437 reduction of electron-accepting functional groups in HS was performed according to
438 Lovley et al. (18). Slurry samples ($\sim 500 \mu\text{l}$) were taken from microcosms with a disposable
439 syringe while bottles were being manually shaken inside an anaerobic chamber. A portion
440 of each sample (200 μl) was mixed with an equal volume of an acidic solution (HCl, 0.5 M)
441 and allowed to stand for 30 min, while the same volume of sample was reacted with ferric
442 citrate (20 mM) for 3 hours. After reaction with ferric citrate, samples were mildly re-
443 suspended in a vortex and 200 μl were left repose with the same volume of HCl solution for
444 30 min. Afterwards, each sample was centrifuged for 10 min at 10,000 g in a centrifuge
445 Spectrafuge 16M and 200 μl of supernatant were then recovered and reacted with a solution
446 0.2 g l^{-1} of 2,4,6-tris(2-pyridil)-1,3,5-triazine (ferrozine reagent). Ferrous iron produced due
447 to chemical reduction of ferric citrate by reduced functional groups in HS, forms a purple
448 complex along with ferrozine reagent, which has its maximum absorbance at 562 nm. The
449 ferrozine solution was buffered with HEPES (50 mM). Once centrifuged samples were

450 mixed with ferrozine solution, they were left reacting for 10 min before their measurement
451 in a spectrometer Thermo Scientific Genesis 10 UV located inside an anaerobic chamber.
452 All solutions employed in this determination were bubbled with N₂ for 30 min to ensure the
453 absence of dissolved oxygen.

454 **Total carbon (TC), total organic carbon (TOC) and total inorganic carbon (TIC)**

455 **measurements.** Water samples were filtered through 0.22 µm nitrocellulose membranes
456 and diluted with deionized water, while sediment samples were dried until constant weight.
457 Both liquid and solid samples were analyzed in a Total Organic Carbon analyzer Shimadzu
458 TOCVCS/TNM-1 equipped with a solids sampling port (SSM-5000A). Solid sample
459 processing time was 6 min at 900°C using O₂ (500 ml min⁻¹) with a purity of 99.9% as
460 carrier gas, all samples were analyzed by triplicate.

461 **Total, volatile and fixed solids.** Total, fixed and volatile solids were measured by triplicate
462 according to Standard Methods procedure (44).

463 **Elemental composition.** Elemental composition of sediments was assessed by analyzing
464 acid-extracts from 2 g of wet sediment. In the case of iron and manganese measurements in
465 microcosms, supernatant samples were taken with disposable syringes, filtered and
466 acidified prior analysis. Samples were then analyzed by inductively coupled plasma optical
467 emission spectrometry (ICP-OES) in an equipment Varian 730-ES. The operational
468 conditions were: potency 1 kW, auxiliary flow: 1.5 l min⁻¹, net flow: 0.75 l min⁻¹, sample
469 taking delay: 30 s, and the number of measured replicates by sample was three. Argon was
470 employed as carrier gas.

471 **DNA extraction, PCR amplification and sequencing.** One microcosm for each selected
472 treatment was randomly chosen at the end of the incubation period (30 days for
473 experiments presented in Fig. 1, and 151 days for experiments depicted in Fig. 6). Before
474 DNA extraction, liquid medium was decanted and extracted from the serological bottles.
475 The total sediment was homogenized afterwards and a subsample of 0.5 g was taken to
476 proceed with DNA extraction. The remaining sediment and the other microcosms were
477 used for material characterization. The total DNA was extracted from sediment samples
478 using the Power Soil DNA extraction kit (MO BIO Laboratories, Carlsbad, CA, USA)
479 following the protocol described by the manufacturer. DNA isolated from each sample was
480 amplified using primers 341F and 785R, targeting the V3 and V4 regions of the 16S rRNA
481 gene fused with Illumina adapter overhang nucleotide sequences (47). The polymerase
482 chain reactions (PCRs) were performed in 50 µl reactions using Phusion Taq polymerase
483 (Thermo Scientific, USA) under the following conditions: denaturation at 98 °C for 60 s,
484 followed by 5 cycles of amplification at 98 °C for 60 s, 50 °C for 30 s and 72 °C for 30 s,
485 followed by 25 cycles of amplification at 98 °C for 60 s, 55 °C for 30 s and 72 °C for 30 s,
486 followed by a final extension of 72 °C for 5 min. Two independent PCR reactions were
487 performed for each sample. The products were indexed using Illumina's 16S Metagenomic
488 Sequencing Library Preparation protocol and Nextera XT Index Kit v2 (Illumina, San
489 Diego CA). Libraries were deep sequenced with the Illumina MiSeq sequencer.

490 **Bioinformatics Analysis.** An analysis of 16S rRNA gene libraries was carried out using
491 Mothur open source software package (v 1.34.4) (48). The high quality sequence data were
492 analyzed for potential chimeric reads using the UCHIME algorithm. Sequences containing
493 homopolymer runs of 9 or more bases, those with more than one mismatch to the

494 sequencing primer and Q-value average below 25 were eliminated. Group membership was
495 determined prior to the trimming of the barcode and primer sequence. Sequences were
496 aligned against the SILVA 123 16S/18S rRNA gene template using the nearest alignment
497 space termination (NAST) algorithm, and trimmed for the optimal alignment region. A
498 pairwise distance matrix was calculated across the non-redundant sequence set, and reads
499 were clustered into operational taxonomic units (OTUs) at 3% distance using the furthest
500 neighbor method. The sequences and OTUs were categorized taxonomically using
501 Mothur's Bayesian classifier and the SILVA 123 reference set. The sequences obtained
502 have been submitted to NCBI GeneBank database.

503 **Accession numbers**

504 The accession numbers of sequences in this work were deposited in the GenBank sequence
505 read archive under the BioProject with SRP094593 accession number.

506 **Acknowledgements**

507 We thank Derek R. Lovley, Jim A. Field, Alfons Stams, Frederic Thalasso, Cesar Nieto and
508 Sonia Arriaga for the discussion. We are also grateful with Matthew Tippett for proof-
509 reading the manuscript. This work was financially supported by grants from the Council of
510 Science and Technology of Mexico (Program Frontiers in Science, grant 1289) and Marcos
511 Moshinsky Foundation to FJC. We thank Dulce Partida, Ma. Carmen Rocha-Medina,
512 Guadalupe Ortega-Salazar, Mariela Bravo-Sánchez, Roberto Camposeco, Elizabeth Cortez
513 and Guillermo Vidriales, for technical support, as well as Lluvia Korynthia López-Aguiar
514 and Yessica Parera-Valadez for their help during sediment collection expeditions. We thank
515 Vicente Rodríguez for access to Cary 5000 UV-Vis spectrophotometer. We are also

516 grateful for the use of infrastructure of the National laboratories LINAN and LANBAMA
517 at IPICYT, as well as USMB at UNAM.

518

519 **References**

520 1. **Reeburgh WS.** 2007. Oceanic methane biogeochemistry. *Chem Rev* **107**:486–513.

521 2. **Boetius A, Ravensschlag K, Schubert CJ, Rickert D, Widdel F, Gieseke A, Amann R,**
522 **Jørgensen BB, Witte U, Pfannkuche O.** 2000. A marine microbial consortium apparently
523 mediating anaerobic oxidation of methane. *Nature* **407**:623–626.

524 3. **Raghoebarsing A, Pol a, van de Pas-Schoonen K, Smolders A, Ettwig K, Rijpstra W,**
525 **Schouten S, Damste J, Op den Camp H, Jetten M, Strous M.** 2006. A microbial
526 consortium couples anaerobic methane oxidation to denitrification RID B-9395-2011 RID
527 F-5114-2011 RID B-8834-2011. *Nature* **440**:918–921.

528 4. **Deutzmann JS, Stief P, Brandes J, Schink B.** 2014. Anaerobic methane oxidation coupled
529 to denitrification is the dominant methane sink in a deep lake. *Proc Natl Acad Sci U S A*
530 **111**:18273–18278.

531 5. **Ettwig KF, Butler MK, Le Paslier D, Pelletier E, Mangenot S, Kuypers MMM,**
532 **Schreiber F, Dutilh BE, Zedelius J, de Beer D, Gloerich J, Wessels HJCT, van Alen T,**
533 **Luesken F, Wu ML, van de Pas-Schoonen KT, Op den Camp HJM, Janssen-Megens**
534 **EM, Francoijs K-J, Stunnenberg H, Weissenbach J, Jetten MSM, Strous M.** 2010.
535 Nitrite-driven anaerobic methane oxidation by oxygenic bacteria. *Nature* **464**:543–8.

536 6. **Beal EJ, House CH, Orphan VJ.** 2009. Manganese- and iron-dependent marine methane
537 oxidation. *Science* **325**:184–7.

538 7. **Egger M, Rasigraf O, Sapart CJ, Jilbert T, Jetten MSM, Röckmann T, Van Der Veen**

- 539 **C, Bânda N, Kartal B, Ettwig KF, Slomp CP.** 2015. Iron-mediated anaerobic oxidation of
540 methane in brackish coastal sediments. *Environ Sci Technol* **49**:277–283.
- 541 8. **Ettwig KF, Zhu B, Speth D, Keltjens JT, Jetten MSM, Kartal B.** 2016. Archaea catalyze
542 iron-dependent anaerobic oxidation of methane. *Proc Natl Acad Sci* **113**:12792–12796.
- 543 9. **Walter Anthony KM, Macintyre S.** 2016. Nocturnal escape route for marsh gas. *Nature*
544 **535**:363–365.
- 545 10. **Bridgham SD, Cadillo-Quiroz H, Keller JK, Zhuang Q.** 2013. Methane emissions from
546 wetlands: biogeochemical, microbial, and modeling perspectives from local to global scales.
547 *Glob Chang Biol* **19**:1325–46.
- 548 11. **Megonigal JP, Hines ME, Visscher PT.** 2004. Anaerobic Metabolism: Linkages to Trace
549 Gases and Aerobic Processes. *Biogeochemistry* 317–424.
- 550 12. **Segarra KE a., Schubotz F, Samarkin V, Yoshinaga MY, Hinrichs K-U, Joye SB.** 2015.
551 High rates of anaerobic methane oxidation in freshwater wetlands reduce potential
552 atmospheric methane emissions. *Nat Commun* **6**:7477.
- 553 13. **Segarra KEA, Comerford C, Slaughter J, Joye SB.** 2013. Impact of electron acceptor
554 availability on the anaerobic oxidation of methane in coastal freshwater and brackish
555 wetland sediments. *Geochim Cosmochim Acta* **115**:15–30.
- 556 14. **Martinez CM, Alvarez LH, Celis LB, Cervantes FJ.** 2013. Humus-reducing
557 microorganisms and their valuable contribution in environmental processes. *Appl Microbiol*
558 *Biotechnol* **97**:10293–308.
- 559 15. **Lehmann J, Kleber M.** 2015. The contentious nature of soil organic matter. *Nature* **528**:60–
560 8.

- 561 16. **Blodau C, Deppe M.** 2012. Humic acid addition lowers methane release in peats of the Mer
562 Bleue bog, Canada. *Soil Biol Biochem* **52**:96–98.
- 563 17. **Miller KE, Lai CT, Friedman ES, Angenent LT, Lipson DA.** 2015. Methane suppression
564 by iron and humic acids in soils of the Arctic Coastal Plain. *Soil Biol Biochem* **83**:176–183.
- 565 18. **Lovley DR, Coates JD, Blunt-Harris EL, Phillips EJP, Woodward JC.** 1996. Humic
566 Substances as Electron acceptors for Microbial Respiration. *Nature*.
- 567 19. **Scott DT, Mcknight DM, Blunt-Harris EL, Kolesar SE, Lovley DR.** 1998. Quinone
568 moieties act as electron acceptors in the reduction of humic substances by humics-reducing
569 microorganisms. *Environ Sci Technol* **32**:2984–2989.
- 570 20. **Straub KL, Benz M, Schink B.** 2000. Iron metabolism in anoxic environments at near
571 neutral pH. *FEMS Microbiol Ecol* **34**:181–186.
- 572 21. **Timmers PH, Suarez-Zuluaga DA, van Rossem M, Diender M, Stams AJ, Plugge CM.**
573 2015. Anaerobic oxidation of methane associated with sulfate reduction in a natural
574 freshwater gas source. *ISME J* **10**:1–13.
- 575 22. **Saxton MA, Samarkin VA, Schutte CA, Bowles MW, Madigan MT, Cadieux SB, Pratt
576 LM, Joye SB.** 2016. Biogeochemical and 16S rRNA gene sequence evidence supports a
577 novel mode of anaerobic methanotrophy in permanently ice-covered Lake Fryxell,
578 Antarctica. *Limnol Oceanogr* **61**:S119–S130.
- 579 23. **Alperin, M. J. RWS.** 1988. Carbon and hydrogen isotope fractionation resulting from
580 anaerobic methane oxidation. *Biogeochem Cycles* **2**:279–288.
- 581 24. **Martens CS, Albert DB, Alperin MJ.** 1999. Stable isotope tracing of anaerobic methane
582 oxidation in the gassy sediments of Eckernförde Bay German Baltic Sea. *Am J Sci* **299**:
583 589–610.

- 584 25. **Socrates G.** 2004. Infrared and Raman characteristic group frequencies
585 characteristic group frequencies.
- 586 26. **Orphan VJ, House CH, Hinrichs K-U, McKeegan KD, DeLong EF.** 2002. Multiple
587 archaeal groups mediate methane oxidation in anoxic cold seep sediments. *Proc Natl Acad*
588 *Sci* **99**:7663–7668.
- 589 27. **Scheller S, Yu H, Chadwick GL, Meglynn SE.** 2016. Artificial electron acceptors
590 decouple archaeal methane oxidation from sulfate reduction. *Science (80-)* **351**:703–707.
- 591 28. **Xi B, Zhao X, He X, Huang C, Tan W, Gao R, Zhang H, Li D.** 2016. Successions and
592 diversity of humic-reducing microorganisms and their association with physical-chemical
593 parameters during composting. *Bioresour Technol* **219**:204–211.
- 594 29. **Coates JD, Cole KA, Chakraborty R, Connor SMO, Achenbach LA.** 2002. Diversity
595 and ubiquity of bacteria capable of utilizing humic substances as electron donors for
596 anaerobic respiration diversity and ubiquity of bacteria capable of utilizing humic substances
597 as electron donors for anaerobic respiration. *Appl Environ Microbiol* **68**:2445–2452.
- 598 30. **Lovley DR, Fraga JL, Blunt-Harris EL, Hayes LA, Phillips EJP, Coates JD.** 1998.
599 Humic substances as a mediator for microbially catalyzed metal reduction. *Acta Hydrochim*
600 *Hydrobiol* **26**:152–157.
- 601 31. **Benz M, Schink B, Brune A.** 1998. Humic acid reduction by *Propionibacterium*
602 *freudenreichii* and other fermenting bacteria. *Appl Environ Microbiol* **64**:4507–4512.
- 603 32. **Glass JB, Yu H, Steele J a, Dawson KS, Sun S, Chourey K, Pan C, Hettich RL, Orphan**
604 **VJ.** 2014. Geochemical, metagenomic and metaproteomic insights into trace metal
605 utilization by methane-oxidizing microbial consortia in sulphidic marine sediments. *Environ*
606 *Microbiol* **16**:1592–611.

- 607 33. **Knittel K, Lösekann T, Boetius A, Kort R, Amann R, Lo T.** 2005. Diversity and
608 Distribution of Methanotrophic Archaea at Cold Seeps Diversity and Distribution of
609 Methanotrophic Archaea at Cold Seeps †. *Appl Environ Microbiol* **71**:467–479.
- 610 34. **Schubert CJ, Vazquez F, Lösekann-Behrens T, Knittel K, Tonolla M, Boetius A.** 2011.
611 Evidence for anaerobic oxidation of methane in sediments of a freshwater system (Lago di
612 Cadagno). *FEMS Microbiol Ecol* **76**:26–38.
- 613 35. **Yoshinaga MY, Lazar CS, Elvert M, Lin YS, Zhu C, Heuer VB, Teske A, Hinrichs KU.**
614 2015. Possible roles of uncultured archaea in carbon cycling in methane-seep sediments.
615 *Geochim Cosmochim Acta* **164**:35–52.
- 616 36. **Biddle JF, Lipp JS, Lever MA, Lloyd KG, Sørensen KB, Anderson R, Fredricks HF,**
617 **Elvert M, Kelly TJ, Schrag DP, Sogin ML, Brenchley JE, Teske A, House CH, Hinrichs**
618 **K-U.** 2006. Heterotrophic Archaea dominate sedimentary subsurface ecosystems off Peru.
619 *Proc Natl Acad Sci U S A* **103**:3846–3851.
- 620 37. **Evans PN, Parks DH, Chadwick GL, Robbins SJ, Orphan VJ, Golding SD, Tyson GW.**
621 2015. Methane metabolism in the archaeal phylum Bathyarchaeota revealed by genome-
622 centric metagenomics. *Science* **350**:434–8.
- 623 38. **Keller, Jason K. & Medvedeff C, A.** 2016. Soil organic matter, p. 165–188. *In* Wetland
624 soils: genesis, hydrology, landscapes, and classifications Vepraskas,. Taylor and Francis
625 Group.
- 626 39. **Pendleton L, Donato DC, Murray BC, Crooks S, Jenkins WA, Sifleet S, Craft C,**
627 **Fourqurean JW, Kauffman JB, Marbà N, Megonigal P, Pidgeon E, Herr D, Gordon D,**
628 **Baldera A.** 2012. Estimating Global “Blue Carbon” Emissions from Conversion and
629 Degradation of Vegetated Coastal Ecosystems. *PLoS One* **7**: e43542.

- 630 40. **Gupta V, Smemo KA, Yavitt JB, Basiliko N.** 2012. Active Methanotrophs in Two
631 Contrasting North American Peatland Ecosystems Revealed Using DNA-SIP. *Microb Ecol*
632 **63**:438–445.
- 633 41. **Smemo KA, Yavitt JB.** 2007. Evidence for Anaerobic CH₄ Oxidation in Freshwater
634 Peatlands. *Geomicrobiol J* **24**:583–597.
- 635 42. **Smemo KA, Yavitt JB.** 2011. Anaerobic oxidation of methane: An underappreciated aspect
636 of methane cycling in peatland ecosystems? *Biogeosciences* **8**:779–793.
- 637 43. **Klüpfel L, Piepenbrock A, Kappler A, Sander M.** 2014. Humic substances as fully
638 regenerable electron acceptors in recurrently anoxic environments. *Nat Geosci* **7**:195–200.
- 639 44. **APHA/AWWA/WEF.** 2012. Standard Methods for the Examination of Water and
640 Wastewater Standard Methods.
- 641 45. **Soga T, Ross GA.** 1999. Simultaneous determination of inorganic anions, organic acids and
642 metal cations by capillary electrophoresis. *J Chromatogr A* **834**:65–71.
- 643 46. **Cord-Ruwisch R.** 1985. A quick method for the determination of dissolved and precipitated
644 sulfides in cultures of sulfate-reducing bacteria. *J Microbiol Methods* **4**:33–36.
- 645 47. **Klindworth A, Pruesse E, Schweer T, Peplies J, Quast C, Horn M, Glöckner FO.** 2013.
646 Evaluation of general 16S ribosomal RNA gene PCR primers for classical and next-
647 generation sequencing-based diversity studies. *Nucleic Acids Res* **41**:1–11.
- 648 48. **Schloss PD, Westcott SL, Ryabin T, Hall JR, Hartmann M, Hollister EB, Lesniewski**
649 **RA, Oakley BB, Parks DH, Robinson CJ, Sahl JW, Stres B, Thallinger GG, Van Horn**
650 **DJ, Weber CF.** 2009. Introducing mothur: Open-source, platform-independent, community-
651 supported software for describing and comparing microbial communities. *Appl Environ*
652 *Microbiol* **75**:7537–7541.

653

654

FIGURE LEGENDS

655 **Fig. 1. Anaerobic methane oxidation measured as $^{13}\text{CO}_2$ production in microcosms'**
656 **headspace and ^{13}C enrichment calculated as $^{13}\text{F}_{\text{CO}_2}$ ($^{13}\text{CO}_2/[^{13}\text{CO}_2 + ^{12}\text{CO}_2]$).** Panel a
657 displays the kinetics for incubations performed with unamended sediment. Panel b displays
658 the kinetics for incubations performed with sediment enriched with 2.5 g l⁻¹ of external
659 NOM in the form of Pahokee Peat humic substances. Error bars represent the standard error
660 among replicates (n = 4, or 3*). SR-INH stands for sediment incubations performed with
661 molybdate (25 mM) in order to inhibit sulfate reduction. $^{13}\text{CO}_2$ production rates were based
662 on the maximum slope observed on linear regressions considering at least three sampling
663 points.

664

665

666 **Fig. 2. Production of $^{13}\text{CO}_2$ and reduction of intrinsic or added electron acceptors at**
667 **the end of the exponential phase (20 days of incubation) in the absence (Panels a and**
668 **b) and in the presence (Panels c and d) of external NOM as HS from Pahokee Peat.**
669 SR-INH stands for controls amended with sulfate-reduction inhibitor, sodium molybdate
670 (25 mM). Error bars represent the standard error among replicates. $^{13}\text{CO}_2$ produced was
671 measured as described for Fig.1. Quantification of sulfate and nitrate reduction imply
672 decrease on their concentration at this sampling time, whereas Fe(III) reduction was
673 quantified in terms of the ferrous iron produced. Reduction of NOM and HS was
674 determined by the ferrozine technique.

675

676 **Fig. 3. Spectroscopic evidence of the presence of quinone moieties and their reduction**
677 **in wetland sediment samples.** Panels a and b depict the Micro-ATR-FTIR representative
678 spectra taken from imaged areas generated after processing quinone functional groups
679 ($1650\text{-}1620\text{ cm}^{-1}$) of sediment samples before incubation in the absence and in the presence,
680 respectively, of external NOM in the form of Pahokee Peat HS. Panels c and e portray XPS
681 high resolution profiles of C1s, while d and f represent O1s signal. Panels c and d belong to
682 sediment samples prior incubation, while panels e and f correspond to sediment samples
683 after incubation with ^{13}C -methane. Regions and components were corrected at 284.8 eV for
684 the C-C adventitious carbon A; B and G components belong to C-O bond (~ 286.6 and ~ 532
685 eV), C and H correspond to C=O functional group (~ 288.9 and ~ 533.3 eV), D belongs to –
686 COOH (~ 289.6), E is typical of the presence of carbonate (~ 291) and F suggests the
687 occurrence of a metallic oxide (~ 530).

688

689 **Fig. 4. High performance Ultraviolet-Visible-Near Infrared spectra obtained from**
690 **liquid samples before and after incubation with $^{13}\text{CH}_4$.** Panels a and c depict spectra
691 obtained before incubation with $^{13}\text{CH}_4$, while panels b and d show spectra obtained after
692 incubation with $^{13}\text{CH}_4$.

693

694 **Fig. 5. Archaeal composition in wetland sediment samples performing AOM.** Most
695 abundant archaeal genera detected, based on 16S rRNA amplicon gene libraries, on

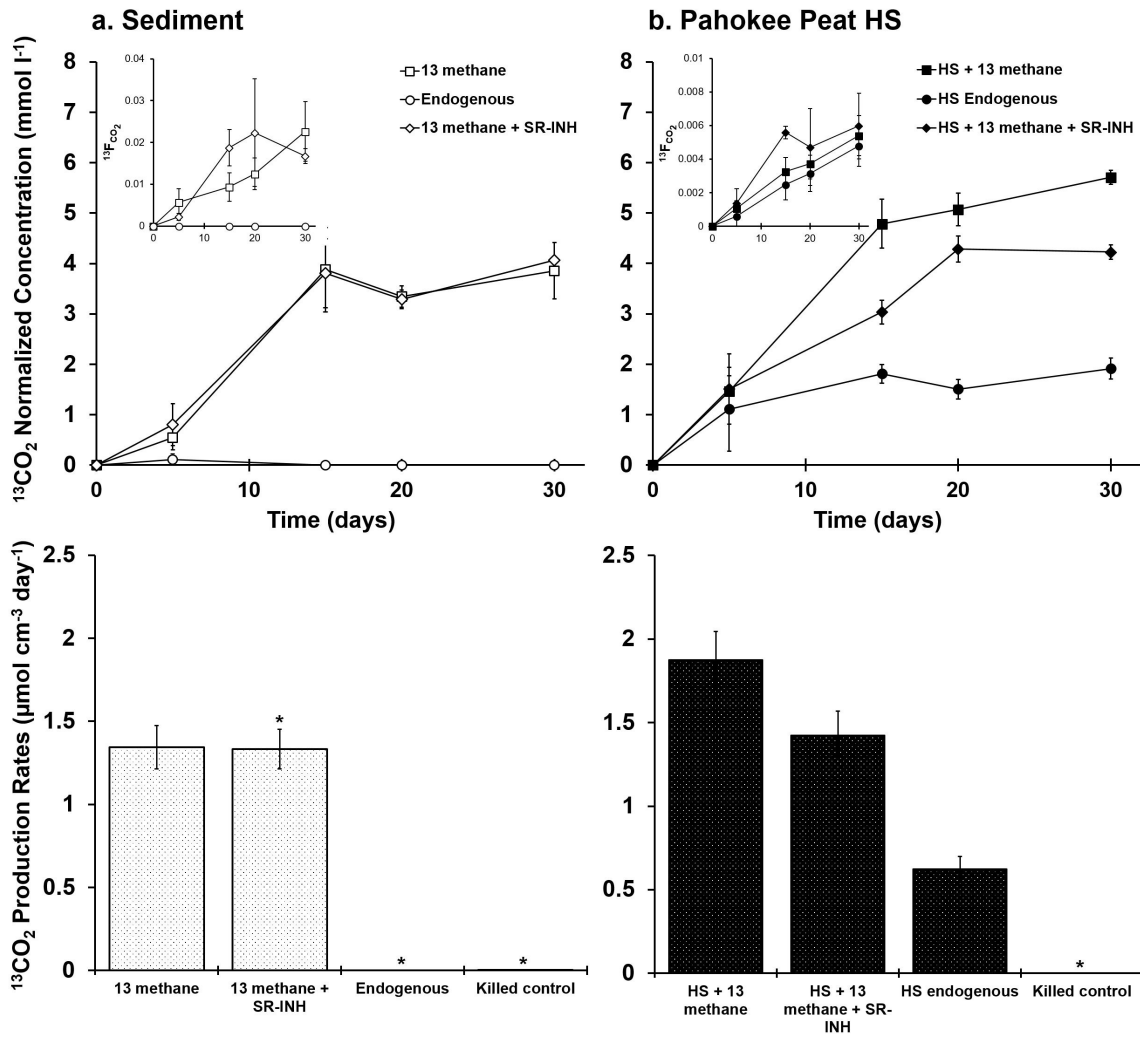
696 selected experimental treatments shown in Fig. 1 at the end of the incubation period (30
697 days).

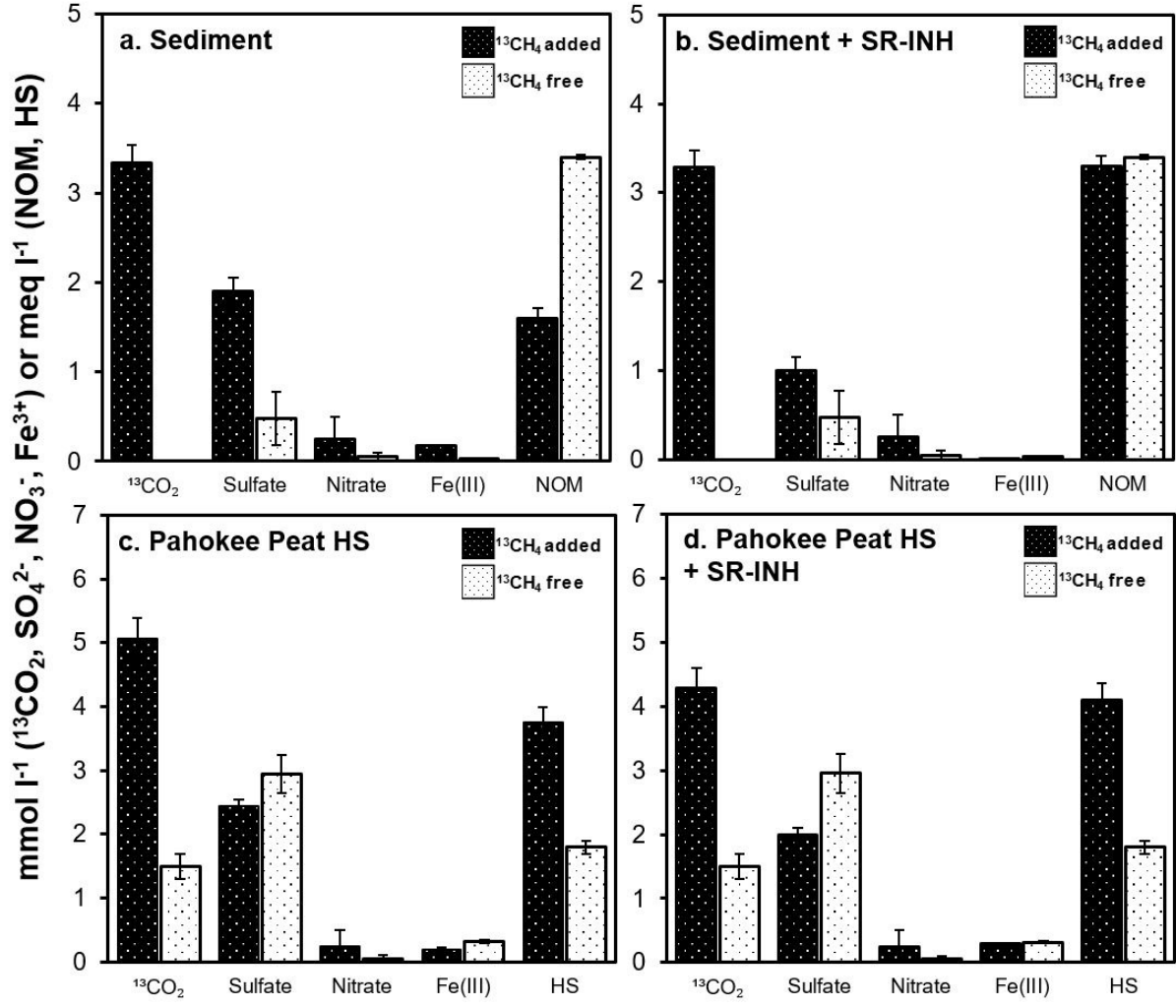
698 **Fig. 6. AOM with AQDS as electron acceptor by an enrichment derived from wetland**
699 **sediment.** Panel a: Kinetics of methane consumption linked to AQDS reduction (to
700 AH_2QDS) observed during the last 11 days of the entire enrichment process lasting 151
701 days: filled squares (-■-) represent microcosms including CH_4 as electron donor and AQDS
702 as electron acceptor (complete experiments, $n=3$), open squares (-□-) represent controls
703 without electron acceptor provided (without AQDS control, $n=3$), solid circles (-●-)
704 represent CH_4 free microcosms (endogenous controls, $n=3$), and crosses (-×-) represent heat
705 killed controls (sterile controls, $n=2$). Error bars represent the standard error among
706 replicates. Panels b and c depict microbial community changes at the end of the enrichment
707 (151 days of incubation) at the phylum level based on Illumina sequencing of 16S rRNA
708 V3-V4 regions. Fresh sediment composition was used as a reference.

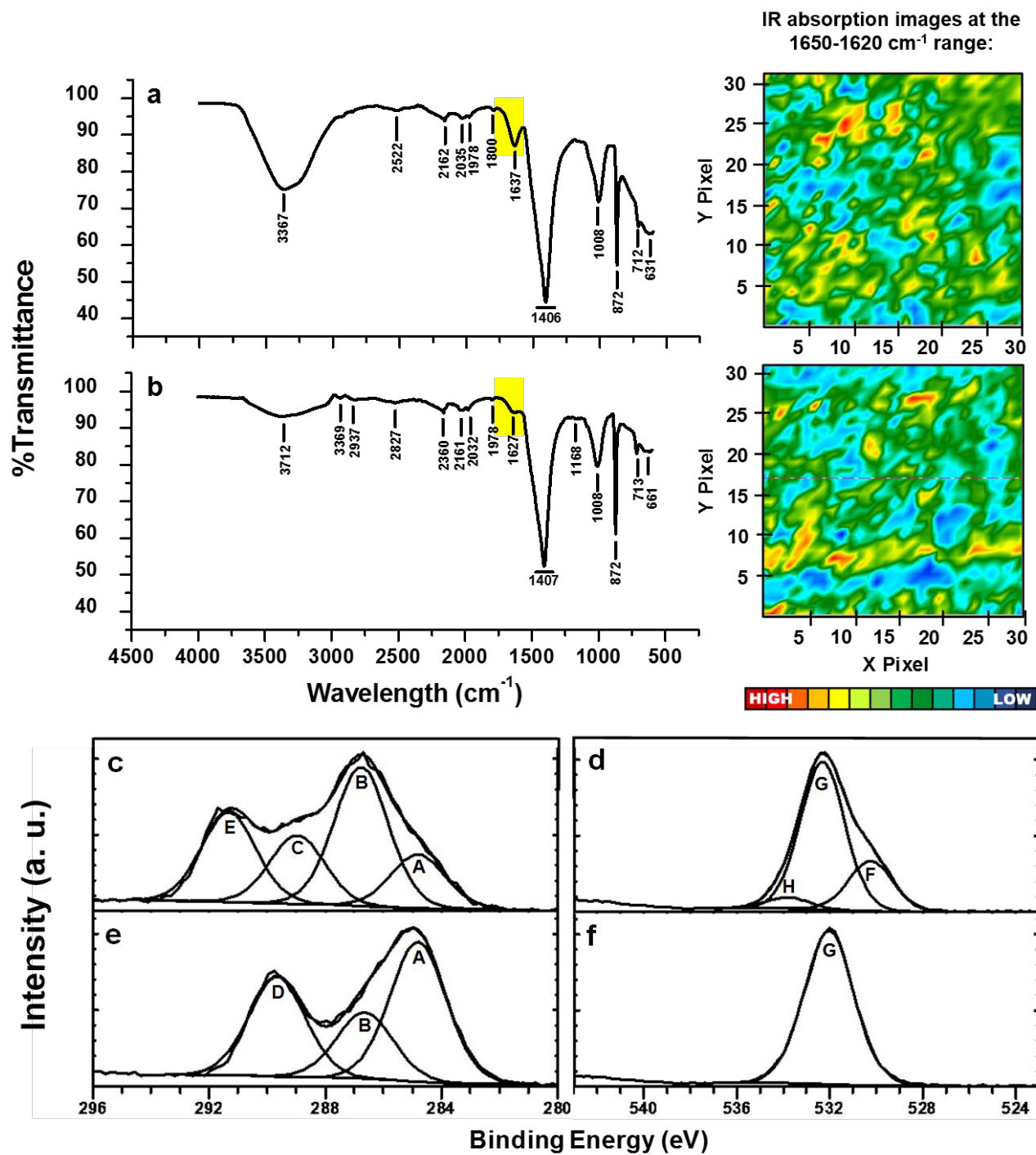
709

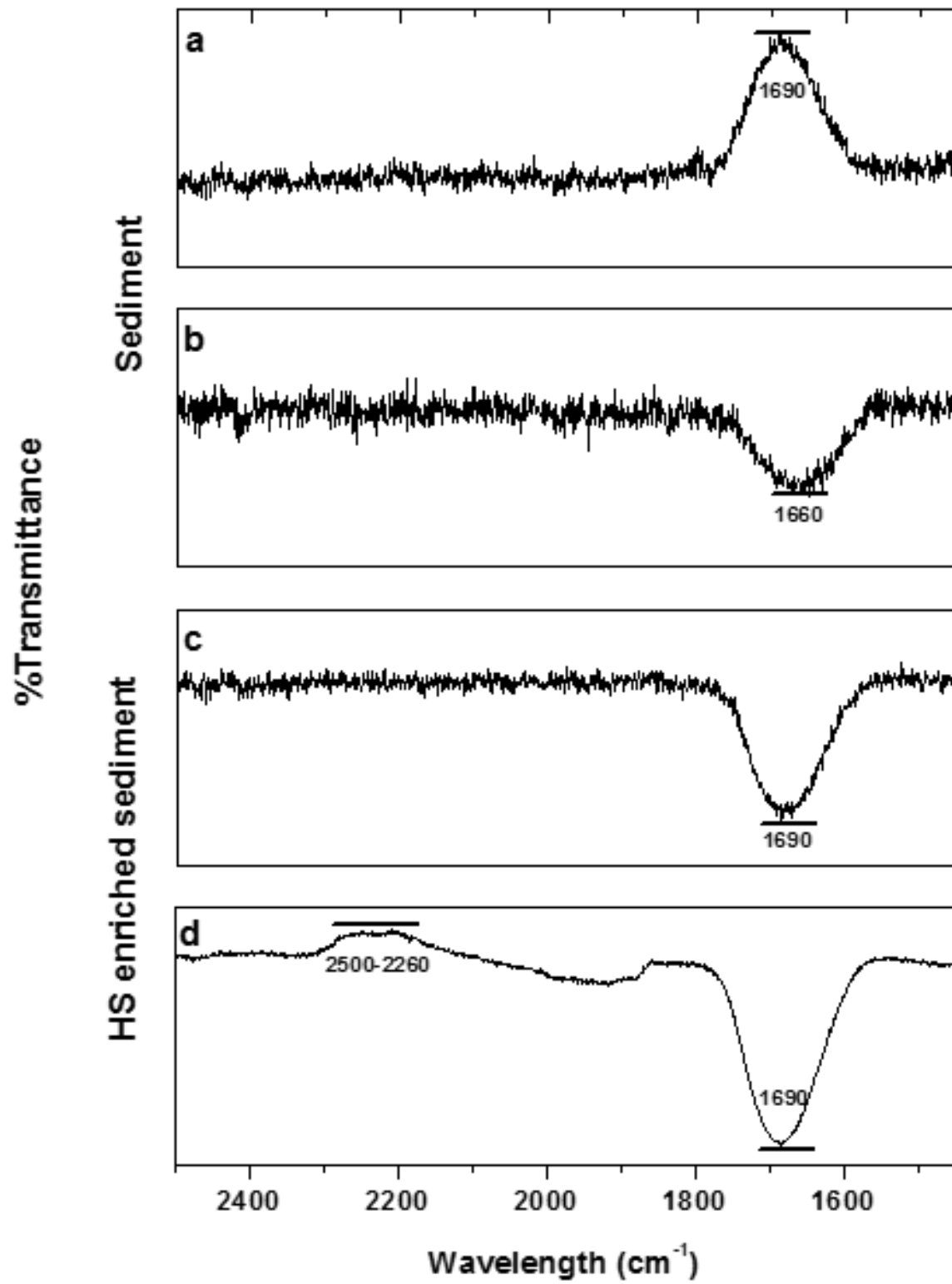
710 **Figure 7. Schematic representation of methane generation and consumption by**
711 **wetland sediment biota.** While a fraction of NOM may serve as electron acceptor to
712 support AOM (NOM-AOM) and decouple sulfate-reduction dependent AOM (SR-AOM),
713 depending on its chemical properties, a labile fraction of NOM could also be degraded
714 following the methanogenesis pathway by a fermenting and methanogenic fraction of the
715 consortia. Equilibrium between these three phenomena must be tightly dependent on
716 thermodynamic conditions, concentration of chemical species, and composition of

717 microbial community. *Anaerobic methanotrophic archaea are considered in a broader
718 perspective than ANME clades from *Euryarchaeota* phylum
719



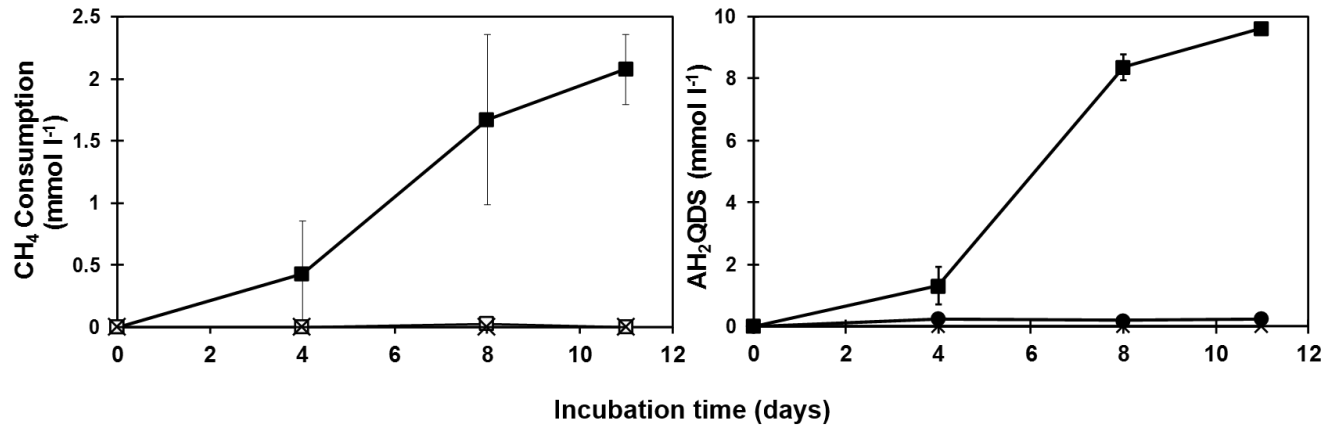
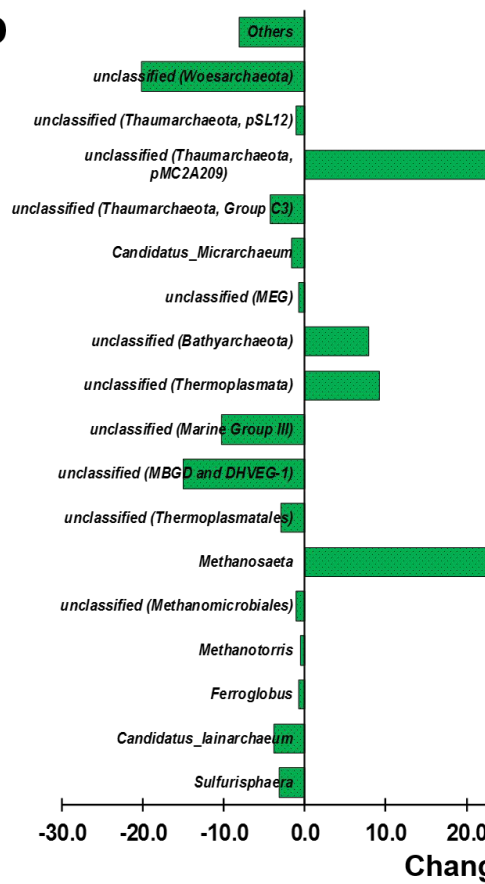






Taxonomy			Treatment				
Phylum	Family	Genus	¹³ C-methane	HS enriched	HS + ¹³ CH ₄	HS + ¹³ C-methane + SR-1NH	
<i>Diapherotrites</i>	Unknown_Family	<i>Candidatus_ Iainarchaeum</i>	0.0	1.1	0.0	1.9	
<i>Euryarchaeota</i>	<i>Halobacteriaceae</i>	<i>Halomarina</i>	0.1	1.4	0.0	0.2	
	ANME 1-b	unclassified (ANME 1-b)	0.0	0.1	0.5	0.0	
	MHLsu47-B8A	unclassified (MHLsu47-B8A)	4.8	2.6	0.1	4.9	
	<i>Methanomicrobiaceae</i>	<i>Methanoculleus</i>	<i>Methanoculleus</i>	0.0	1.2	0.0	0.0
		<i>Methanogenium</i>	<i>Methanogenium</i>	0.2	0.5	1.6	0.4
		<i>Methanomicrobium</i>	<i>Methanomicrobium</i>	2.4	2.4	2.8	2.0
	SMS-sludge-7	unclassified (SMS-sludge-7)	1.1	2.1	0.2	1.2	
	<i>Methanosaetaceae</i>	<i>Methanosaeta</i>	4.0	1.5	3.2	1.3	
	<i>Methanosarcinaceae</i>	ANME-3	0.2	0.0	0.0	0.0	
	Unknown_Family	unclassified (Fe-A-9)	0.5	0.2	0.0	3.5	
	AMOS4A-452-E11	unclassified (AMOS4A-452-E11)	1.4	0.6	0.1	0.9	
Marine_Benthic_Group_D_and_DHVEG-1	unclassified (MBGD and DHVEG-1)	22.6	18.9	20.6	17.7		
Marine_Group_III	unclassified (MG_III)	3.5	1.6	4.9	1.4		
<i>Bathyarchaeota</i>	unclassified	unclassified (<i>Bathyarchaeota</i>)	12.8	7.5	14.0	10.0	
SM1K20	unclassified	unclassified (SM1K20)	0.7	0.4	1.6	0.6	
<i>Thaumarchaeota</i>	unclassified	unclassified (Group_C3)	3.9	2.6	2.7	2.1	
	unclassified	unclassified (MBGB)	6.6	5.6	11.9	4.9	
	unclassified	unclassified (pMC2A209)	19.3	16.3	14.9	12.5	
<i>Woesearchaeota</i> _(DHVEG-6)	unclassified	unclassified (DHVEG-6)	11.7	26.2	15.6	25.0	
	Others	Others	4.3	7.0	5.4	9.4	



a**b****c**